http://dx.doi.org/10.5935/0103-5053.20150244

J. Braz. Chem. Soc., Vol. 27, No. 2, 303-313, 2016.
Printed in Brazil - ©2016 Sociedade Brasileira de Química
0103 - 5053 $6.00+0.00

Article

Synthesis and Characterization of Mesoporous Nb_2O_5 and Its Application for Photocatalytic Degradation of the Herbicide Methylviologen

Douclasse C. Castro, Rodrigo P. Cavalcante, Juliana Jorge, Marco A. U. Martines, Lincoln C. S. Oliveira, Gleison A. Casagrande and Amilcar Machulek Jr.*

Instituto de Química, Universidade Federal de Mato Grosso do Sul, Av. Senador Filinto Müller, 1555, CP 549, 79074-460 Campo Grande-MS, Brazil

This article reports the characterization of mesoporous Nb_2O_5 synthesized by the sol-gel method for application in photocatalysis. The emerging contaminant methylviologen was employed for photocatalytic tests. Parameters inherent to the synthesis process, such as stirring rate, aging temperature, and calcination temperature, were employed for a range of values to improve the synthetic route. The powders obtained were characterized by thermogravimetric analysis, X-ray diffraction, scanning and transmission electron microscopy, specific surface area, infrared spectroscopy, energy-dispersive spectroscopy, and diffuse reflectance spectroscopy. In samples calcined at 450 °C, a mixture of amorphous and hexagonal phases was observed, with a predominance of the former, while in samples calcined at 650 °C the orthorhombic phase predominated. Samples calcined at 450 °C exhibited larger specific surface areas. Mesoporous structures were confirmed for samples T8035M450 and T8045mi450, which displayed higher photoactivity, with roughly 90% removal of methylviologen.

Keywords: advanced oxidation processes, photocatalysis, sol-gel method, mesoporous Nb_2O_5, methylviologen

Introduction

The expansion of intensive farming around the world and the large-scale development of the agrochemical industry in response to the growing demand for food, have led to a drastic increase in the amount and variety of pesticides in surface water and groundwater.[1,2] Pesticides are responsible for most of the effluents containing high concentrations of toxic non-biodegradable compounds not amenable to removal by conventional water treatment.[3,4] Pesticide management has been an issue of major concern in scientific circles, given the potential environmental impact of these compounds.[2]

In Brazil, the demand for pesticides has been increasing year by year, and the country is currently one of the largest consumers of these products. According to the Brazilian Union of Plant Defensive Industries (SINDIVEC),[5] the domestic agrochemical market grew by 6-9% in 2014. Of the pesticides employed in crop production, herbicides have become the most used. Reasons for this increase include the expansion of planted areas and the diffusion of agricultural technologies. In Brazil, herbicides represented 19% of pesticide sales in 2013, accounting for US$ 3.739 billion.[5]

Among numerous emerging contaminants, paraquat, also known as methylviologen (MV^{2+}), a non-selective contact herbicide of the bipyridyl class (dimethyl-4,4'-bipyridinium dichloride), was first marketed in 1962. Its low cost and high effectiveness have placed it among the most widely employed herbicides in crops such as rice, coffee, sugarcane, beans and soybeans in over 130 countries.[6-8]

Toxicity and persistence make pesticides a serious environmental concern,[1] it is necessary to introduce additional technologies to suitably remove these compounds from effluents. Advanced technologies have recently been used in the treatment of effluents containing multiple compounds, and advanced oxidation processes (AOPs) have gained particular attention for their ability to successfully remove persistent organic compounds.[9-14]

By means of physical and chemical mechanisms that produce powerful transitional species, particularly hydroxyl radicals ($HO^{\bullet}$), of high oxidative power, AOPs can efficiently destroy a wide range of highly toxic organic compounds impervious to conventional technologies, converting recalcitrant contaminants into more easily

*e-mail: machulekjr@gmail.com

biodegradable, less toxic compounds and/or fully mineralizing them into carbon dioxide, water and inorganic anions.[15,16] Among AOPs, heterogeneous photocatalysis has been a focus of interest for its ability to degrade harmful pollutants.[17] The principle underlying heterogeneous processes is the activation of a semiconductor by sunlight or artificial light.[18]

When the surface of the semiconductor material is excited with photons with energy equal or higher than band gap energy (E_{gap}), electrons are promoted from the valence band (VB) to the conduction band (CB). As a result of this, an electron (e^-_{CB}) hole (h^+_{VB}) pair is produced (equation 1).[19]

$$\text{semiconductor} + h\nu \rightarrow e^-_{CB} + h^+_{VB} \quad (1)$$

The positive holes oxidize either pollutant directly (equation 2, pollutant is represented by P) or react with adsorbed species such as water molecules or hydroxide ion to produce $HO^\bullet$ radicals (equation 3).[20] Similarly the electron can be donated to an electron acceptor (oxygen adsorbed) to produce superoxide radical anion, $O_2^{\bullet -}$ (equation 4).[21]

$$h^+_{VB} + P \rightarrow P^+ \quad (2)$$

$$h^+_{VB} + H_2O_{ads} \rightarrow HO^\bullet + H^+ \quad (3)$$

$$e^-_{CB} + O_{2ads} \rightarrow O_2^{\bullet -} \quad (4)$$

Essentially, these reactive transitory species generated ($HO^\bullet$, $O_2^{\bullet -}$, h_{VB}^+, $HO_2^\bullet$) are the main responsible for the degradation of organic pollutants present in the medium. However, a series of secondary reactions (equations 5-8) can occur.[22,23]

$$O_2^{\bullet -} + H_2O_{ads} \rightarrow H_2O_2 \quad (5)$$

$$H_2O_2 \rightarrow 2HO^\bullet \quad (6)$$

$$h^+_{VB} + HOO^- \rightarrow H_2O_2 \quad (7)$$

$$e^-_{CB} + HOO^- \rightarrow HO_2^- \quad (8)$$

Heterogeneous photocatalysis typically employs transition metal oxides and sulfides (e.g., TiO_2, Fe_2O_3, WO_3, SnO_2, ZnO, Nb_2O_5, CdS or ZnS) that act as photosensitizers in photoinduced processes, owing to electronic structures in which the valence band is semi-filled, while the conduction band remains empty.[24]

Despite the effectiveness of TiO_2, ZnO, and Nb_2O_5 as catalysts,[25] TiO_2[26-30] and ZnO[31-34] are the most employed, owing to their ability to form stable hydrocolloids in aqueous media, facilitating interaction with the compound to be degraded and improving photoactivity.[35] However, because recovery of these semiconductors for reuse is complex and laborious,[36] alternative semiconductors have been viewed as a promising solution to meet the requirements of Green Chemistry Principle No. 7 (use of renewable sources of raw materials).[37]

Despite a band gap energy of 3.4 eV, higher than that of TiO_2 (3.2 eV), Nb_2O_5 has the advantage of not forming a stable hydrocolloid with target compounds. It can thus be easily recovered and reused, without significant loss of photocatalytic activity, which makes it a promising catalyst for use in photocatalysis.[38,39] Because of its acidic nature, Nb_2O_5 is widely used in catalytic reactions such as dehydration, esterification, hydrolysis, condensation, and particularly oxidation reactions. Nonetheless, its photocatalytic properties remain scarcely investigated.[38,40-45]

Roughly 98% of known reserves of niobium are located in Brazil. The country currently accounts for over 90% of all niobium traded worldwide, followed by Canada and Australia.[46] Investigating new technological applications for this metal is therefore highly relevant.

Most industrial processes using Nb_2O_5 as a photocatalyst employ the micrometric form of this material, obtained by calcining the commercial oxide or by treatment with reagents such as hydrogen peroxide, acids, and alkalis,[43] a disadvantage in heterogeneous photocatalysis, since catalyst photoactivity depends directly on physical and chemical properties that include surface area, morphology, mesoporous structure, adsorption capacity, crystal structure, and particle size.[47] The ability to synthesize the catalyst to achieve control of properties such as formation of mesoporous structures is therefore of great interest.

The principal approaches for synthesizing nanostructures are the sol-gel, polymer precursor, hydrothermal, and solvothermal methods.[48] The sol-gel method has long been used to produce porous materials exhibiting large surface areas.[39] Molecular precursors, especially metal alkoxides, are commonly employed, owing to their high purity and ease of control of the synthesis process.[49,50] Conversion of an alkoxide into a gel occurs by precipitation followed by hydrolysis and condensation (with polymerization of the hydrolyzed species).[51]

The purpose of this study was to characterize mesoporous Nb_2O_5 photocatalysts synthesized by the sol-gel method, considering their use in photocatalysis and employing MV^{2+} as a model emerging contaminant. The oxides thus synthesized were characterized by thermogravimetric analysis (TGA/DTG), X-ray diffraction

(XRD), scanning and transmission electron microscopy (SEM and TEM), specific surface area (BET), Fourier-transform infrared spectroscopy (FTIR), energy dispersive spectroscopy (EDS), and diffuse reflectance spectroscopy (DRS).

Experimental

Reagents

All reagents were of analytical grade. MV^{2+} (98%) was purchased from Sigma Aldrich, isopropyl alcohol (99.8%) from Merck, surfactant Tween 80 (polyoxyethylene (20) sorbitan monooleate, $C_{64}H_{124}O_{26}$) from Synth, and niobium(V) chloride from Companhia Brasileira de Metalurgia e Mineração (CBMM).

Synthesis of mesoporous Nb_2O_5

Nb_2O_5 nanoparticles were synthesized by the sol-gel method from the niobium(V) isopropoxide, as adapted from the procedure described by Antonelli *et al.*[52] Synthesis was performed by hydrolysis, followed by condensation of the alkoxide and aging under constant stirring and controlled temperature. The route employed has the advantage of eliminating the need for chelating agents.

As a first step, niobium isopropoxide ($C_{15}H_{35}NbO_5$) was synthesized. In a glovebox with nitrogen atmosphere, 1.89 g of niobium(V) chloride ($NbCl_5$) was dissolved in 10 g of isopropyl alcohol (equation 9). The reaction system was kept under constant stirring for 40 min until all $NbCl_5$ dissolved. To evaluate the formation of $C_{15}H_{35}NbO_5$, the product obtained was characterized by hydrogen nuclear magnetic resonance (NMR).

$$NbCl_5 + 5\,(CH_3)_2CHOH \rightarrow Nb((OCH)(CH_3)_2)_5 + 5\,HCl\uparrow \quad (9)$$

The synthesized niobium isopropoxide was mixed with 0.3 g of Tween 80 surfactant under stirring and 1.8 mL of ultrapure water was then added. The resultant mixture was left to age for 72 h. The precipitate was separated by centrifugation (4500 rpm for 30 min), washed with ultrapure water, dried, and calcined at ambient temperature. Two oxides, synthesized in the absence of surfactant, served as blanks.

Synthesis conditions (aging temperature, stirring speed, calcination temperature) have a pronounced effect on the physicochemical properties of products (e.g., phase, morphology, particle size, specific surface area) and consequently on their photocatalytic properties, and were therefore investigated (Table 1).

Table 1. Variables investigated in the synthesis of mesoporous Nb_2O_5 by the sol-gel method

Surfactant	Aging temperature / °C	Stirring speed	Calcination temperature / °C	Catalyst code
Tween 80	35	mi[a]	450	T8035mi450
Tween 80	35	M[b]	450	T8035M450
Tween 80	45	mi[a]	450	T8045mi450
Tween 80	45	M[b]	450	T8045M450
Tween 80	35	mi[a]	650	T8035mi650
Tween 80	35	M[b]	650	T8035M650
Tween 80	45	mi[a]	650	T8045mi650
Tween 80	45	M[b]	650	T8045M650
No additional treatment			450	B450[c]
No additional treatment			650	B650[c]

[a]mi: minimum (50% stirring); [b]M: maximum (100% stirring); [c]B: blank.

Characterization

The surface morphology and surface topography of samples were examined using a JSM-7100F scanning electron microscope and a JEM-2100 transmission electron microscope (both from Jeol). For SEM, the samples were mounted on carbon tape and sputter-coated with platinum. For TEM, the samples were dispersed in ethanol with the aid of ultrasound and deposited onto copper grids. Mean diameter of particles was determined by counting the particles shown in TEM images from different fields in each sample, using ImageJ software.[53]

For qualitative analysis of the elemental composition of the synthesized material, EDS measurements were performed using a JSM-6830LV scanning electron microscope (Jeol) with a 30 kV electron beam.

For thermogravimetry, the samples were placed in a platinum crucible and analyzed on a TGA Q50 device (TA Instrument) (heating rate: 10 °C min^{-1}; temperature range: 25-900 °C; nitrogen atmosphere, with flow rates of 40 mL min^{-1} in the thermobalance and 60 mL min^{-1} in the furnace). The crystal structures of powders were investigated by analyzing XRD from 4 to 100° (2θ) at 0.017° intervals and measuring time of 50 s $step^{-1}$, employing an X'pert PRO MRD diffractometer (PANalytical) as the Cu Kα radiation source (λ = 1.5406 Å). Specific surface area, pore volumes, and pore size distributions were determined by nitrogen adsorption analysis, based on BET isotherms. The samples were degassed at 150 °C for 15 h and measurements were taken at 77 K. UV-Vis diffuse reflectance electronic spectra of the powders were obtained using a pulsed PX2 xenon lamp and a USB-4000 detector (both from Ocean Optics), optical

fibers, and Ocean Optics SpectraSuite software. Magnesium oxide was used as the reference for total reflection. Scans were performed at 250-800 nm. FTIR spectra were recorded using an MB spectrophotometer (Bomem), with scanning at 500-4000 cm^{-1}, employing powder dispersion in potassium bromide pellets.

Photodegradation procedures

Photocatalytic efficiency was evaluated by MV^{2+} photodegradation rates. The experiments were conducted in an annular glass photochemical reactor with 1 L capacity and quartz casing for insertion of the radiation source. UV radiation was provided by a 125 W medium-pressure mercury vapor lamp (Philips) of 4.59×10^{21} s^{-1} photon flux experimentally determined by chemical actinometry.[12,27] The lamp, without its protective casing, was positioned lengthways to the reactor, within a quartz tube. A magnetic stirrer homogenized the solution throughout the experiment. The photochemical reactor temperature was monitored throughout the reaction at 25 °C with the aid of a thermostatic bath. For the photodegradation experiments, 0.5 g of the desired catalyst was placed in 500 mL of MV^{2+} solution at 0.2 mmol L^{-1}. The experiments were performed without pH control (pH ca. 6.0 ± 0.2). Reaction time was 100 min and aliquots of approximately 4 mL were collected at predetermined intervals and filtered. Degradation was monitored by absorption spectrophotometry in the UV-Vis range on a U-3000 UV-Vis spectrophotometer (Hitachi).

Results and Discussion

Characterization results

^1H NMR analysis was performed to confirm the presence of niobium isopropoxide (a precursor of Nb_2O_5 synthesis), formed by reacting $NbCl_5$ with isopropanol. The isopropanol spectrum (Figure 1a) shows three characteristic regions around 0.9, 3.7, and 4.2 ppm, corresponding to a carbon doublet, a sextet, and hydroxyl, respectively. In the spectrum shown in Figure 1b, the band corresponding to the hydroxyl group, at 4.2 ppm, disappears, owing to replacement of a hydrogen with a niobium atom (see equation 9), confirming the formation of niobium isopropoxide. The presence of niobium (a paramagnetic atom) causes the neighboring hydrogen atoms to relax, which translates to the spectral changes observed at 3.7 and 4.2 ppm.

The thermal behavior of the synthesized oxides was investigated by monitoring the removal, during TGA/DTG analysis, of adsorbed water and the organic matter originating from isopropanol and surfactant. This technique was also employed as a pre-step for selecting the calcination temperature range to be employed in the synthetic route.

All materials synthesized exhibited similar behaviors. Figure 2 shows the profile of mass loss as a function of temperature and its derivative for the synthesized oxide, for an aging temperature of 45 °C and minimum stirring speed. Three major stages can be observed. The first spans the

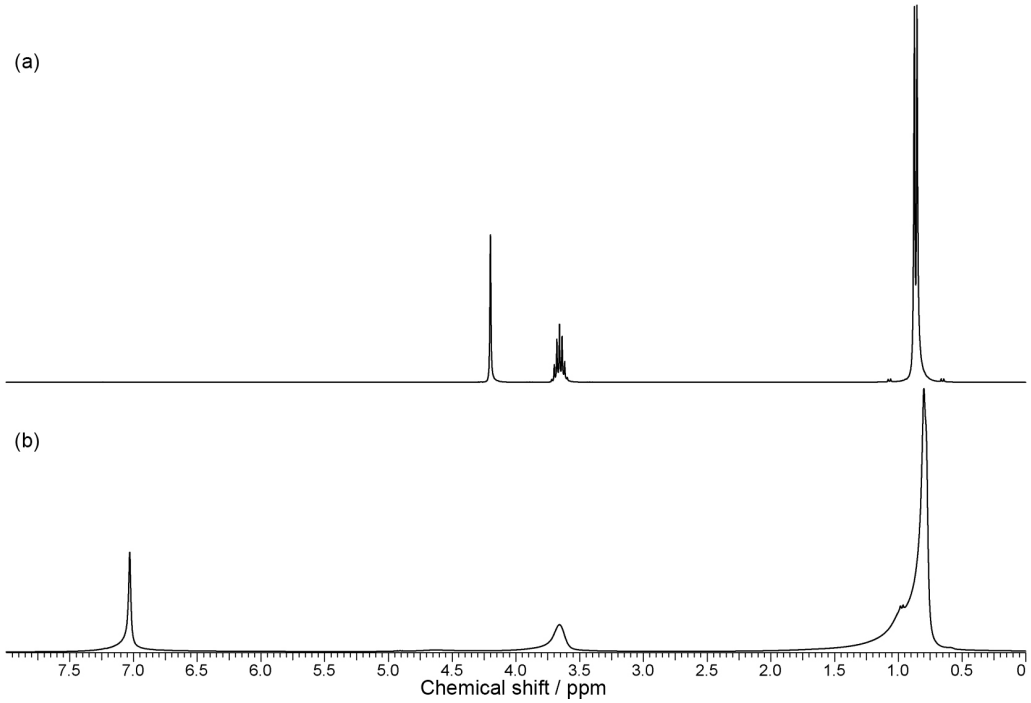

Figure 1. ^1H NMR spectrum (300 MHz, $CDCl_3$) for (a) isopropanol; (b) niobium isopropoxide.

50-100 °C region, with a 9.41% mass loss corresponding to removal of surface water, as well as isopropyl alcohol, since organic residues are often present in samples synthesized by the sol-gel method.[54] The second, in the 100-300 °C range accounted for a mass loss of 7.99%, attributed to decomposition of organic matter, surfactant, and niobium isopropoxide and one last step in the region of 300-560 °C attributed to removal of organics adsorbed on the surface and to structural arrangement of the oxide. On the DTG curve, the first step is supported by two exothermic peaks at about 50 and 100 °C, while the second step is supported by four peaks, at about 230, 479, and 554 °C, showing that thermodecomposition involves more steps than indicated by the TGA curve. Throughout the analysis, mass loss was about 19% of the initial mass, with 81% of the residue consisting of Nb_2O_5.

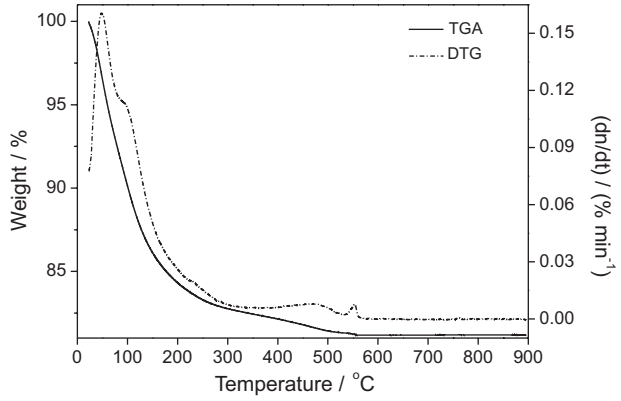

Figure 2. TGA/DTG curves for the sample synthesized at an aging temperature of 45 °C, with minimum stirring.

XRD was employed to examine the changes occurring in the crystal structures of the oxides (Figure 3). As expected, the oxides synthesized via the controlled route in the presence of surfactant exhibited lower crystallinity than samples B450 or B650 (as revealed by the high intensity of the majority of dominant diffraction peaks of these samples), possibly because the controlled parameters imparted relatively well-organized atomic arrangements to the synthesized materials, hence their low crystallinity.

The diffractograms of samples calcined at 450 °C (Figure 3a) revealed a mixture of hexagonal and predominantly amorphous phases, the latter confirming the presence of mesoporous particles. All wide-angle peaks in both patterns correspond to a pure TT-phase (JCPDS, 28-317), with major peaks indexed as (001), (100), (101), (002), (110), (102), (111), (200), (201), (112), and (202), respectively. These results reveal similarities with TT-phase samples, according to parameters published by Schaffer *et al.*[55] Other investigators also obtained an amorphous phase by calcining at 400-500 °C.[56-59]

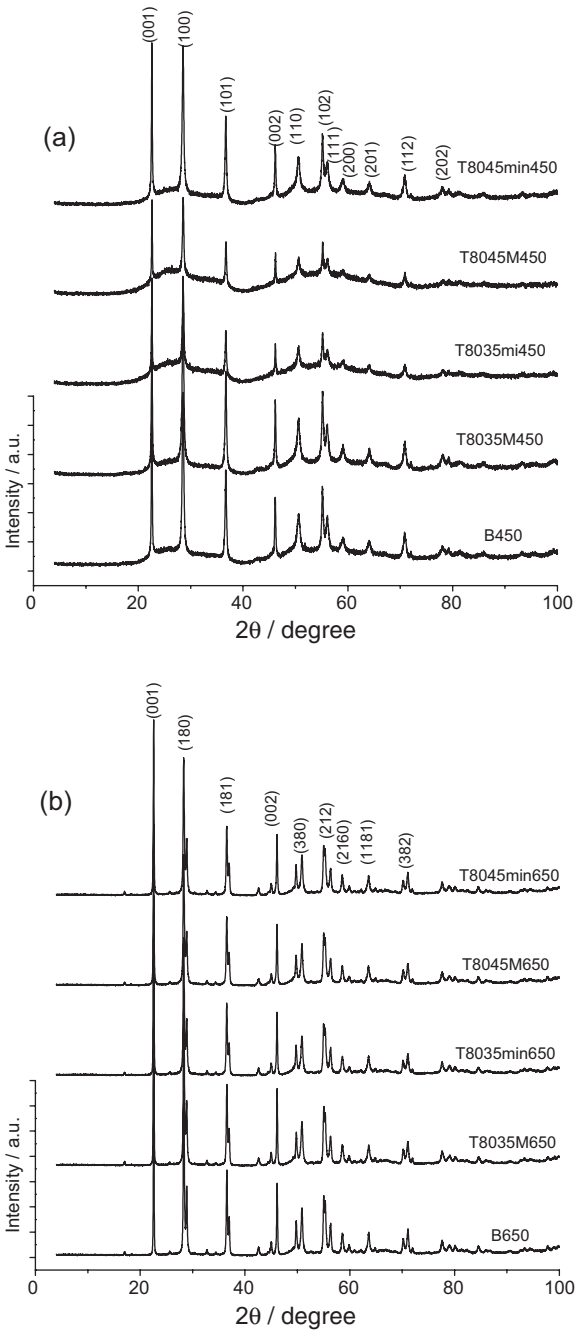

Figure 3. Diffractograms of photocatalysts calcined at (a) 450 °C; (b) 650 °C.

For a higher calcination temperature (650 °C, Figure 3b), peaks attributed to the orthorhombic phase[55] were observed, with major peaks indexed as (001), (180), (181), (002), (380), (212), (202), (2160), (1181), and (382), respectively.[56,59-63]

Nb_2O_5 crystal size (Table 2) was estimated from the position and height of peak (001) using the Debye-Scherrer equation-namely, $D = 0.89\ \lambda/(\beta \cos\theta)$. Crystal size increased with rising calcination temperatures, ranging from 74.44 to 111.65 nm.

Table 2 shows the BET surface areas (S_{BET}) and pore volumes (V_p) of the synthesized oxides. Calcination temperature affects area-to-mass values, as shown by the lower surface area values obtained for the catalysts calcined at 650 °C. Semiconductors with larger surface areas tend to provide better photocatalytic responses.[64] A reduction in surface areas with increasing temperatures has also been observed elsewhere.[58,65-67] Maurer and Ko[67] found that a decrease in surface area with increasing calcination temperature corresponded to changes in the crystal phase of Nb_2O_5-results consistent with our XRD data. In oxides synthesized under maximum stirring speed and calcined at 450 °C, increasing aging temperatures caused S_{BET} and V_p values do diminish. Also, all the oxides calcined at 450 °C exhibited higher S_{BET} and V_p values than oxide B450.

Pores with diameters of 2 to 50 nm are known to correspond to mesoporous materials.[68] For oxides T8035M450 and T8045mi450, pore diameters of 6.60 and 4.10 nm were obtained, respectively, and their nitrogen adsorption-desorption isotherms were consistent with typical patterns for mesoporous materials (Type IV, in the IUPAC classification of adsorption isotherms), indicating the mesoporous nature of these materials.[69] For the other synthesized oxides, no isotherms typical of mesoporous materials were observed. Figure 4 compares typical isotherms of a mesoporous (T8035M450) and a non-mesoporous sample (T8035M650), confirming the closure of pores with increasing temperatures.

Table 2. Characterization of the photocatalysts investigated

Photocatalyst	S_{BET}[a] / (m^2 g^{-1})	V_p[b] / (cm^3 g^{-1})	Crystal size[c] / nm
B450	12.4 ± 0.2	0.05	74.4
T8035M450	74.4 ± 1.0	0.10	81.2
T8035mi450	48.8 ± 0.9	0.08	81.2
T8045M450	28.4 ± 0.2	0.06	74.4
T8045mi450	49.2 ± 0.8	0.07	81.2
B650	7.2 ± 0.1	0.04	111.6
T8035M650	10.6 ± 0.1	0.06	111.6
T8035mi650	10.1 ± 0.2	0.06	89.3
T8045M650	9.8 ± 0.2	0.08	89.3
T8045mi650	11.0 ± 0.2	0.07	89.3

[a]BET surface areas (S_{BET}), measured by the BET method; [b]pore volumes (V_p) obtained from the volume of N_2 adsorbed at $P/P_0 = 0.98$; [c]measured from XRD data using the Debye-Scherrer equation.

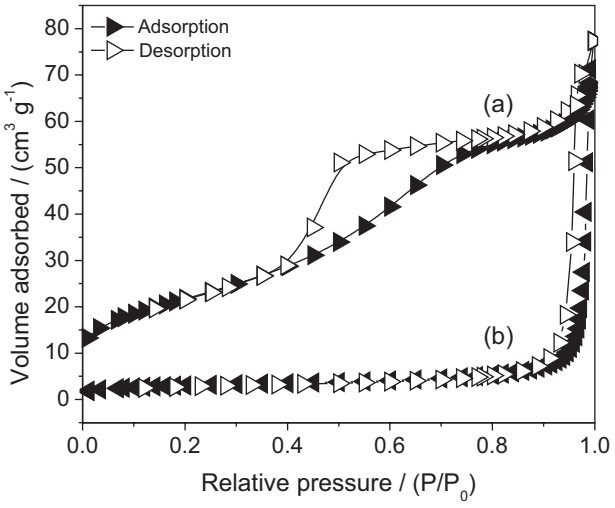

Figure 4. N_2 adsorption-desorption isotherms for samples (a) T8035M450; (b) T8035M650.

Band gap energy (E_{gap}) values were estimated by linear regression of the absorption slope by extrapolating the tangent to the energy ($E = 1240.82/\lambda$) *vs*. absorbance curve obtained from DRS experiments. Figure 5 shows the behavior of absorbance, from which the E_{gap} value was determined for T8035M450 sample. E_{gap} values of the other photocatalysts were determined in the same manner. For all the synthetic routes, the estimated E_{gap} values remained within the 3.0-3.1 eV range-consistent with published values of 3.08-3.20 eV,[56] 3.22 eV,[60] and 2.99-3.17 eV.[70] The synthesized oxides can therefore be employed as UV-Vis radiation-absorbing materials.

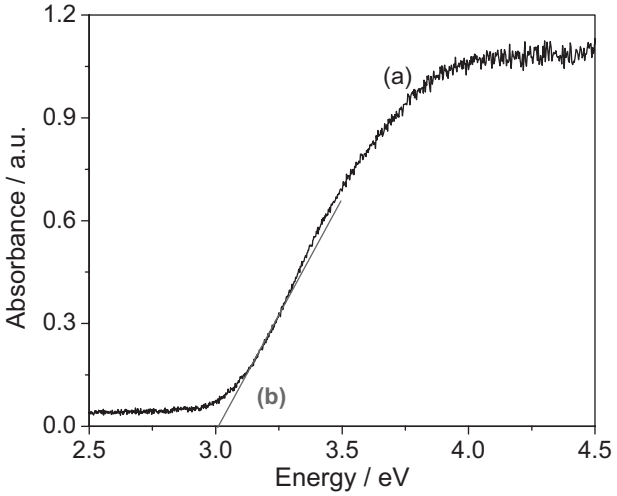

Figure 5. (a) Absorbance; (b) linear regression, as a function of energy (eV) for determining the energy band gap value of T8035M450.

All the oxides were subjected to infrared spectroscopy to monitor the removal of adsorbed water and organic matter (such as surfactant) that takes place during calcination, as well as the formation of oxide polymer networks. All spectra exhibited similar peaks. Figure 6 shows the curves corresponding to the infrared spectra obtained before and after heat treatment at 450 °C of the sample synthesized under maximum stirring and aging temperature of 35 °C.

In the FTIR spectra, Nb_2O_5 formation is corroborated by the presence of a strong, broad band around 620 cm^{-1},

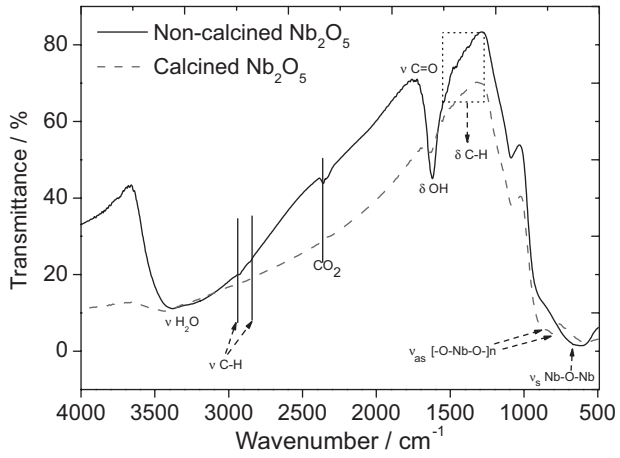

Figure 6. FTIR spectrum (KBr) of Nb_2O_5 before and after heat treatment.

attributed to symmetric stretching of Nb–Nb–O bonds,[71,72] and bands around 810 and 867 cm^{-1}, corresponding to asymmetric stretching of $[–O–Nb–O]_n$ bonds.[73]

Surfactant and water removal can be confirmed by the absence of bands in the calcined sample-namely, (*i*) 3376 cm^{-1}, corresponding to OH stretching resulting from polymer association, (*ii*) 3660 and 1620 cm^{-1}, corresponding to stretching and angular deformation, respectively, of water molecules adsorbed onto the material, and (*iii*) 1296 cm^{-1} (C=O), 2918 cm^{-1} (ν C–H), and 1450 cm^{-1} (δ CH out of plane), for C–H and ester bonds of the surfactant.[74]

Sample constituents were confirmed by EDS. FTIR confirmed the presence of niobium and oxygen in all synthesized oxides, demonstrating formation of Nb_2O_5.

With the aid of SEM data, the effect of variations in the synthetic routes on particle morphology in the oxides was evaluated. Figure 7 shows SEM images of samples B450 and B650, revealing that oxides consisted of particle clusters with a rounded morphology. Figure 7a, for sample B450, reveals that TiO_2 particles are constituted of clusters. Clusters of these types are smaller, more aggregated, and more defined than in oxide B650 (Figure 7b), indicating the influence of the calcination temperature on particle morphology. These results are consistent with surface areas, since the clusters are closer together in the oxides synthesized at 650 °C, resulting in smaller surface areas.

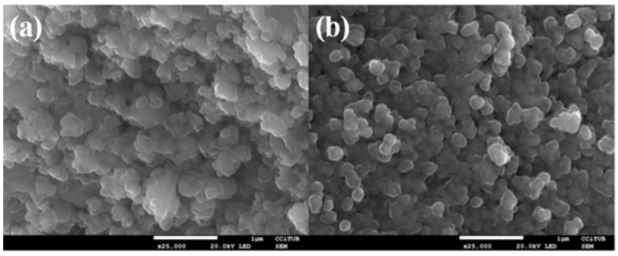

Figure 7. SEM images of samples (a) B450; (b) B650.

Particles exhibited better-defined shapes in the oxides calcined at 650 °C (Figures 8 and 9), demonstrating the effect that surfactant presence during synthesis has on particle morphology, as well as the influence of modifying the parameters investigated.

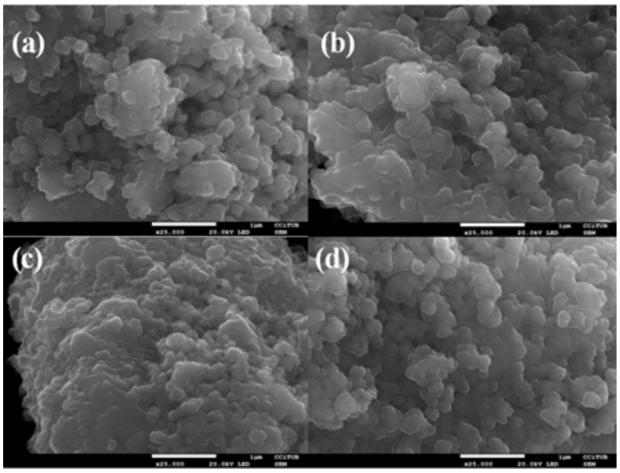

Figure 8. SEM images of samples (a) T8035mi450; (b) T8035M450; (c) T8045mi450; (d) T8045M450.

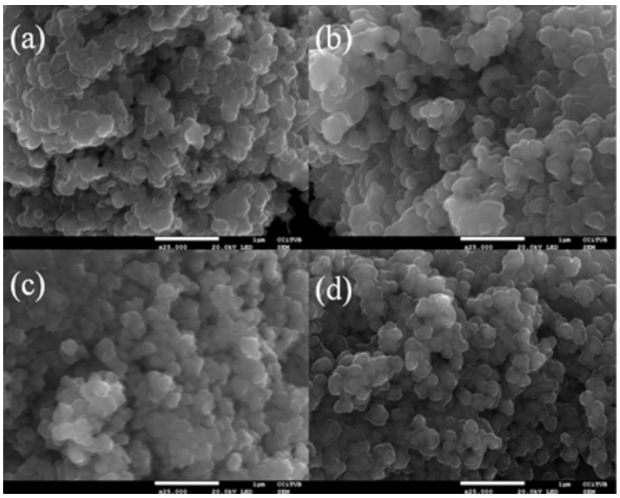

Figure 9. SEM images of samples (a) T8035mi650; (b) T8035M650; (c) T8045mi650; (d) T8045M650.

It is observed that oxides synthesized employing an aging temperature of 45 °C exhibited more pronounced clustering, but increased stirring speed produced more dispersed particles, albeit not uniformly organized. This lack of uniformity is typical of the surfactant used as a template, i.e., the micelles formed in its presence are not uniformly organized.

Figure 10 shows representative TEM images and histograms of particle size distributions (estimated using Feret diameters) for mesoporous sample T8035M450 and non-mesoporous sample T8045M450. Because Nb_2O_5 particles are polydisperse, their dimensions could not be

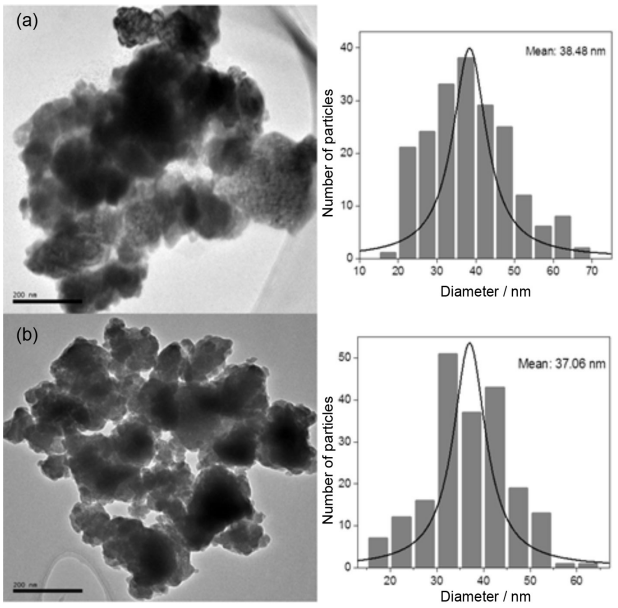

Figure 10. TEM images and particle distribution of samples (a) T8035M450; (b) T8045M450.

correctly determined, but most ranged from 30 to 50 mm in both samples. Also, sample T8035M450 was found to have a mesoporous structure, as shown by the N_2 adsorption-desorption isotherms and TEM images.

Investigation of photocatalytic efficiency, based on methylviologen photodegradation

The photocatalytic activities of the obtained Nb_2O_5 nanoparticles were investigated in MV^{2+} degradation (0.2 mmol L^{-1} of MV^{2+} and 1.0 g L^{-1} of catalyst). The results of photodegradation experiments are shown in Figure 11a.

This study was employed to evaluate changes in physicochemical properties resulting from changes in synthesis parameters (presence of surfactant, aging temperature, stirring speed, calcining temperature).

Direct photolysis was insufficient to degrade MV^{2+}, with only 58% of MV^{2+} was degraded after 100 min under UV radiation with medium-pressure mercury vapor lamp (Philips, photon flux = 4.59×10^{21} s^{-1}). Even the MV^{2+} has a very strong UV signal at 257 nm that corresponds to a π-π* transition of the electrons in the pyridinium ring[75] and consequently, overlaying the spectrum of the incoming radiation (maximum intensity at 254 nm), its removal was inefficient. On the other hand, more than 90% of MV^{2+} was degraded within 60 min using oxides T8035M450 and T8045mi450.

To quantify differences between degradation rates, MV^{2+} oxidation rate data were employed to calculate k_{ap}, the pseudo-first-order kinetic constant (Table 3) from the regression line slopes representing $-\ln(MV^{2+}/MV^{2+}_o)$ *vs.* time (Figure 11b).

As can be seen (Figure 11a and Table 3), the highest degradation rates (between 92 to 88%) were obtained with oxides calcined at 450 °C, in agreement with Paulis *et al.*,[58] who found a strong relationship between calcining temperature and catalytic activity of Nb_2O_5. These results were corroborated by the results of characterization, in which the oxides exhibited higher surface areas and mesoporous structures, both of which account for superior photocatalytic activity.

Another explanation for the improved photocatalytic response of oxides calcined at 450 °C is that the surfaces of oxides calcined at this temperature contain Brønsted-Lowry acid centers, and increasing the calcination temperature converts these active centers into Lewis acids.[58] Because Lewis acids are electron-deficient[76] and MV^{2+} in aqueous solution is positively charged, these conditions may have interfered with the interaction

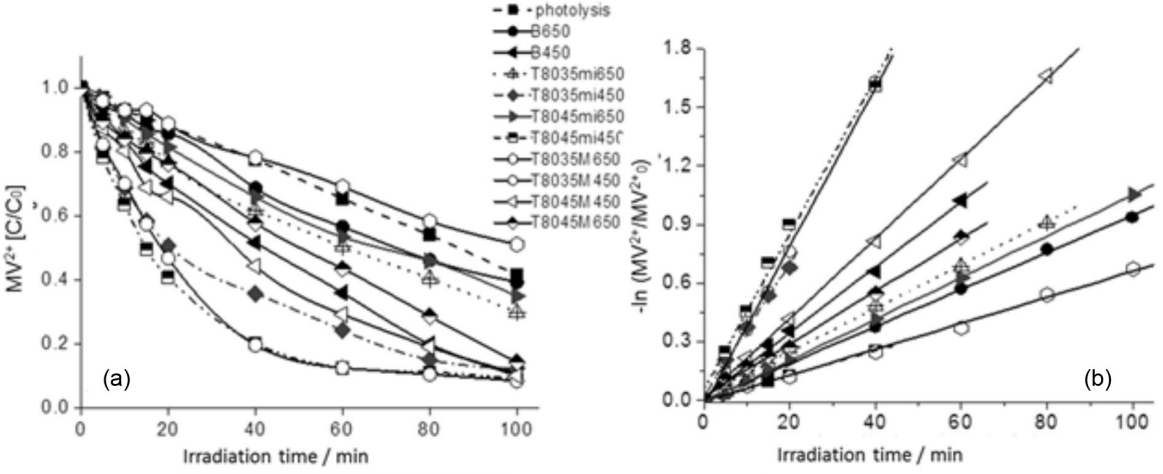

Figure 11. Methylviologen degradation curves; $[MV^{2+}]_0$ = 0.02 mmol L^{-1}; [catalyst] = 0.5 g *per* 500 mL.

Table 3. Methylviologen removal percentages and respective pseudo-first-order kinetic constants

Photocatalyst	Degradation / %	k_{ap}[a] / min^{-1}	R
Photolysis	58	0.63×10^{-2}	0.999
B450	89	1.65×10^{-2}	0.998
T8035M450	92	4.08×10^{-2}	0.998
T8035mi450	88	3.38×10^{-2}	0.997
T8045M450	90	2.05×10^{-2}	0.999
T8045mi450	91	3.98×10^{-2}	0.997
B650	61	0.95×10^{-2}	0.999
T8035M650	49	0.66×10^{-2}	0.998
T8035mi650	70	1.11×10^{-2}	0.999
T8045M650	86	1.34×10^{-2}	0.998
T8045mi650	65	1.06×10^{-2}	0.999

[a]Pseudo-first-order kinetic constant (k_{ap}).

between substrate and catalyst surface, lowering catalytic efficiency.

Results of MV^{2+} degradation using oxides calcined at 450 °C showed that the aging temperature and stirring speed did not influence in the photocatalytic efficiency of catalysts.

Degradation rates decreased significantly for the oxides calcined at 650 °C (see Table 3), probably owing to the higher crystallinity of these materials (as shown by XRD data). Crystallinity considerably decreases the rate of substrate adsorption onto the catalyst surface, consequently reducing photocatalytic response. Unexpectedly, the sample T8045M650 exhibited highest MV^{2+} degradation after 100 min of treatment. One possible explanation could be the fact that the oxide showed lower crystallinity, but to confirm a further study of XRD data would be necessary.

The application of Nb_2O_5 catalyst for the photodegradation of contaminants is few reported in the literature in comparation of TiO_2.

Padro *et al.*[41] synthesized cellulose acetate/Nb_2O_5 catalyst in different proportions of Nb_2O_5 (3.9, 5.8, 6.7 and 10.9 in wt.%) and applied as photocatalyst to degrade indigo carmine dye. The materials showed high quality to degrade indigo carmine dye in aqueous solution, obtaining nearly 100% degradation with the catalyst prepared with 6.7% of Nb_2O_5 in 30 min of reaction. In another study, Prado *et al.*[38] applied commercially available Nb_2O_5 catalyst to degrade indigo carmine dye. The authors investigated the effect of catalyst concentration, pH and ionic strength (μ) and compared with degradation catalyzed by TiO_2 and ZnO. Almost 100% of dye degradation occurred at 90 min.

Silva *et al.*[77] prepared Nb_2O_5 and Ag/Nb_2O_5 with 2 wt.% silver by the impregnation method. For the catalytic tests, the authors prepared solutions of 10 ppm of the following dyes: yellow neutracyl, dark blue neutracyl, blue dispersatyl, orange dispersatyl, black dispersatyl, black neutracyl. The tests carried out with pure niobium oxide showed that the best degradation, 38.14% discoloration, was achieved with black dispersatyl, while the worst degradation, 9.89% discoloration, was obtained with black neutracyl. The presence of silver in the catalyst, Ag/Nb_2O_5, resulted in a better performance of the catalysts, showing over 90% degradation for all dyes.

Hashemzadeh *et al.*[78] synthesized Nb_2O_5 nanoparticles via a hydrothermal process from of the commercial Nb_2O_5 powder and used methylene blue (MB) and rhodamine B (RhB) as contaminant dye in water to study the photocatalytic activities of samples illuminated by visible light. The results showed that after 120 min of irradiation, the MB removal over Nb_2O_5 nanoparticles arrives at 89%, obviously higher than the value of 43% for RhB dye.

Raba *et al.*[79] synthesized Nb_2O_5 via Pechini method and investigated its performance in processes photoinduced of rhodamine B and atrazine degradation, under visible light irradiation. Additionally, the authors studied for three different heat treatments (500 ºC for 2 h, 600 ºC for 2 h, 500 ºC for 11 h in nitrogen flow and 11 h in air flow). The authors obtained 30% of atrazine removal after 50 min for the two oxide tested (samples calcined at 500 ºC without gas flow and with the gas flow). For photocatalytic tests using rhodamine, the oxide of low cost (samples calcined at 500 ºC without gas) was used. The degradation rate for this contaminant was lower compared to atrazine.

According to all the mentioned in the previous paragraphs and by comparison with our results, we can claim that the catalysts presented in this paper have good photocatalytic activity, consequently encourage the use of of these catalysts synthesized as an effective technology for the treatment of MV^{2+}.

Conclusions

Nb_2O_5 synthesized by the sol-gel method is a promising material for the photocatalytic degradation of emerging contaminants, with the advantage of easy removal and recovery, thus overcoming a major obstacle in the use of traditional photocatalysts (TiO_2 and ZnO).

The results showed that choice of a suitable synthetic route is crucial for the synthesis of highly active photocatalysts. Calcination temperature was the synthesis parameter that most influenced photocatalytic response. The highest MV^{2+} removal rates were obtained with oxides calcined at 450 °C, particularly T8035M450 (91% removal) and T8045mi450 (92%). These photocatalytic efficiency results are consistent

with the characterization of these oxides (large surface areas and formation of mesoporous structures, as confirmed by pore diameters and TEM images).

Crystallinity increased with rising calcination temperatures. The more crystalline the oxide, the lower the adsorption of MV^{2+} onto its surface, and consequently the lower the MV^{2+} degradation rate obtained.

Acknowledgements

The authors wish to thank the Brazilian Funding Agencies CNPq (Conselho Nacional de Desenvolvimento Científico e Tecnológico), CAPES (Coordenação de Aperfeiçoamento de Pessoal de Nível Superior), FUNDECT (Fundação de Apoio ao Desenvolvimento do Ensino, Ciência e Tecnologia do Estado de Mato Grosso do Sul) and INCT-EMA (Instituto Nacional de Ciência e Tecnologia de Estudos do Meio Ambiente).

References

1. Orellana-García, F.; Álvarez, M. A.; López-Ramón, V.; Rivera-Utrilla, J.; Sánchez-Polo, M. J.; Mota, A.; *Chem. Eng. J.* **2014**, *255*, 307.
2. Reddy, P. V. L.; Kim, K-H.; *J. Hazard. Mater.* **2015**, *285*, 325.
3. Gozzi, F.; Machulek Jr., A.; Ferreira, V. S.; Osugi, M. E.; Santos, A. P. F.; Nogueira, J. A.; Dantas, R. F.; Esplugas, S.; Oliveira, S. C.; *Chem. Eng. J.* **2012**, *210*, 444.
4. Badawy, M. I.; Ghaly, M. Y.; Gad-Allah, T. A.; *Desalination* **2006**, *194*, 166.
5. SINDIVEG, Sindicato Nacional da Indústria de Produtos para Defesa Vegetal, http://www.sindiveg.org.br/ accessed in September, 2015.
6. Eisler, R.; *Eisler's Encyclopedia of Environmentally Hazardous Priority Chemicals*, 1st ed.; Elsevier: Amsterdan, 2007.
7. Santos, M. S. F.; Alves, A.; Madeira, L. M.; *Chem. Eng. J.* **2011**, *175*, 279.
8. Dhaouadi, A.; Adhoum, N.; *J. Electroanal. Chem.* **2009**, *637*, 33.
9. Machulek Jr., A.; Quina, F. H.; Gozzi, F.; Silva, V. O.; Friedrich, L. C.; Moraes, J. E. F. In *Fundamental Mechanistic Studies of the Photo-Fenton Reaction for the Degradation of Organic Pollutants*; Puzyn, T.; Mostrag-Szlichtyng, A., eds.; Rijeka: InTech, 2012.
10. de Luca, A.; Dantas, R. F.; Simões, A. S. M.; Toscano, I. A. S.; Lofrano, G.; Cruz, A.; Esplugas, S.; *Chem. Eng. Technol.* **2013**, *36*, 2155.
11. de Luca, A.; Dantas, R. F.; Esplugas, S.; *Water. Res.* **2014**, *61*, 232.
12. Cavalcante, R. P.; Sandim, L. R.; Bogo, D.; Barbosa, A. M. J.; Osugi, M. E.; Blanco, M.; Oliveira, S. C.; Matos, M. F. C.; Machulek Jr., A.; Ferreira, V. S.; *Environ. Sci. Pollut. Res.* **2013**, *20*, 2352.
13. Zanta, C. L. P. S.; Friedrich, L. C.; Machulek Jr., A.; Higa, K. M.; Quina, F. H.; *J. Hazard. Mater.* **2010**, *178*, 258.
14. Machulek Jr., A.; Gogritcchiani, E.; Moraes, J. E. F.; Quina, F. H.; Braun, A. M.; Oliveros, E.; *Sep. Purif. Technol.* **2009**, *67*, 141.
15. Andreozzi, R.; Caprio, V.; Insola, A.; Marotta, R.; *Catal. Today* **1999**, *53*, 51.
16. Buxton, G. V.; Greenstock, C. L.; Helman, W. P.; Ross, A. B.; *J. Phys. Chem. Ref. Data* **1988**, *17*, 513.
17. Malato, S.; Fernández-Ibáñez, P.; Maldonado, M. I.; Blanco, J.; Gernjak, W.; *Catal. Today* **2009**, *147*, 1.
18. Klavarioti, M.; Mantzavinos, D.; Kassinos, D.; *Environ. Int.* **2009**, *35*, 402.
19. Rauf, M. A.; Ashraf, S. S.; *Chem. Eng. J.* **2009**, *151*, 10.
20. Ahmed, S.; Rasul, M. G.; Martens, W. N.; Brown, R.; Hashib, M. A.; *Desalination* **2010**, *261*, 3.
21. Kabra, K.; Chaudhary, R.; Sawhney, R. L.; *Ind. Eng. Chem. Res.* **2004**, *43*, 7683.
22. Chong, M. N.; Jin, B.; Chow, C. W. K.; Saint, C.; *Water Res.* **2010**, *44*, 2997.
23. Wang, Y.; He, Y.; Lai, Q.; Fan, M.; *J. Environ. Sci.* **2014**, *26*, 2139.
24. Bahnemann, D.; *Sol. Energy* **2004**, *77*, 445.
25. Lang, X.; Chen, X.; Zhao, J.; *Chem. Soc. Rev.* **2014**, *43*, 473.
26. Romero, V.; De la Cruz, N.; Dantas, R. F.; Marco, P.; Giménez, J.; Esplugas, S.; *Catal. Today* **2011**, *161*, 115.
27. Ramos, D. D.; Bezerra, P. C. S.; Quina, F. H.; Dantas, R. F.; Casagrande, G. A.; Oliveira, S. C.; Oliveira, M. R. S.; Oliveira, L. C. S.; Ferreira, V. S.; Oliveira, S. L.; Machulek Jr., A.; *Environ. Sci. Pollut. Res.* **2015**, *22*, 774.
28. Cavalcante, R. P.; Dantas, R. F.; Bayarri, B.; González, O.; Giménez, J.; Esplugas, S.; Machulek Jr., A.; *Catal. Today* **2015**, *252*, 27.
29. Cavalcante, R. P.; Dantas, R. F.; Bayarri, B.; González, O.; Wender, H.; Giménez, J.; Esplugas, S.; Machulek Jr., A.; *Appl. Catal., B.* **2015**, *176-177*, 173.
30. Méndez-Arriaga, F.; Maldonado, M. I.; Giménez, J.; Esplugas, S.; Malato, S.; *Catal. Today* **2009**, *144*, 112.
31. Zhai, H.; Wang, L.; Sun, D.; Han, D.; Qi, B.; Li, X.; Chang, L.; Yang, J.; *J. Phys. Chem. Solids* **2015**, *78*, 35.
32. Khan, R.; Hassan, M. S.; Uthirakumar, P.; Yun, J. H.; Khil, M.-S.; Lee, I.-H.; *Mater. Lett.* **2015**, *152*, 163.
33. Kaur, J.; Singhal, S.; *Ceram. Int.* **2014**, *40*, 7417.
34. Kazeminezhad, I.; Sadollahkhani, A.; *Mater. Lett.* **2014**, *120*, 267.
35. Hoffmann, M. R.; Martin, S. T.; Choi, W.; Bahnemann, D. W.; *Chem. Rev.* **1995**, *95*, 69.
36. Sarkar, S.; Chakraborty, S.; Bhattacharjee, C.; *Ecotoxicol. Environ. Saf.* **2015**, *in press*, DOI: 10.1016/j.ecoenv.2015.02.035.

37. Lenardão, E. J.; Freitag, R. A.; Dabdoub, M. J.; Batista, A. C. F.; Silveira, C. C.; *Quim. Nova* **2003**, *26*, 123.
38. Prado, A. G. S.; Bolzon, L. B.; Pedroso, C. P.; Moura, A. O.; Costa, L. L.; *Appl. Catal., B* **2008**, *82*, 219.
39. Zhao, Y.; Zhou, X.; Ye, L.; Tsang, S. C. E.; *Nano Rev.* **2012**, *3*, 17631.
40. Kominami, H.; Oki, K.; Kohno, M.; Onoue, S.; Kera, Y.; Ohtani, B.; *J. Mater. Chem.* **2001**, *11*, 604.
41. Prado, A. G. S.; Faria, E. A.; Souza, J. R.; Torres, J. D.; *J. Mol. Catal. A: Chem.* **2005**, *237*, 115.
42. Torres, J. D.; Faria, E. A.; Souza, J. R.; Prado, A. G. S.; *J. Photochem. Photobiol., A* **2006**, *182*, 202.
43. Lopes, O. S.; Paris, E. C.; Ribeiro, C.; *Appl. Catal., B.* **2014**, *144*, 800.
44. Zhang, M.; Hu, C.; He, X.; Wan, B.; Xi, Y.; *Catal. Commun.* **2009**, *11*, 206.
45. Ferrari-Lima, A. M.; Marques, R. G.; Gimenes, M. L.; Fernandes-Machado, N. R. C.; *Catal. Today* **2015**, *254*, 119.
46. http://www.cprm.gov.br/publique/cgi/cgilua.exe/sys/start.htm?infoid=2616&sid=129, accessed in September, 2015.
47. Gálvez, J. B.; Malato, S. R.; Gasca, C. A. E.; Bandala, E. R.; Gelover, S.; Leal, T. In *Purificación de Aguas por Fotocatálisis Heterogénea: Estado del Arte;* Blesa, M. A., ed.; Digital Grafic: La Plata, 2001, ch. 3.
48. Mourão, H. A. J. L.; Mendonça, V. R.; Malagutti, A. R.; Ribeiro, C.; *Quim. Nova* **2009**, *32*, 2181.
49. Karagedov, G.; Feltz, A.; Neidnicht, B.; *J. Mater. Sci.* **1991**, *26*, 6396.
50. Bradley, D. C.; Mehrotra, R. C.; Gaur, D. P.; *Metal Alkoxides*; Academic Press: New York, 1978.
51. Guglielmi, M.; Carturan, G.; *J. Non-Cryst. Solids* **1988**, *100*, 16.
52. Antonelli, D. M.; Nakahira, A.; Ying, J. Y.; *Inorg. Chem.* **1996**, *35*, 3126.
53. Abramoff, M. D.; Magalhaes, P. J.; Ram, S. J.; *Biophotonics Int.* **2004**, *11*, 36.
54. Lambert, C. K.; Gonzalez, R. D.; *Mater. Lett.* **1999**, *38*, 145.
55. Schaffer, H.; Gruehn, R.; Schulte, F.; *Angew. Chem. Int. Ed.* **1966**, *5*, 40.
56. Chen, X.; Yu, T.; Fan, X.; Zhang, H.; Li, Z.; Ye, J.; Zou, Z.; *Appl. Surf. Sci.* **2007**, *253*, 8500.
57. Sarkar, A.; Pramanik, P.; *Microporous Mesoporous Mater.* **2009**, *117*, 580.
58. Paulis, M.; Martín, M.; Soria, D. B.; Díaz, A.; Odriozola, J. A.; Montes, M.; *Appl. Catal., A* **1999**, *180*, 411.
59. Tanaka, M.; Shima, H.; Yokoi, T.; Tatsumi, T.; Kondo, J. N.; *Catal. Lett.* **2011**, *141*, 283.
60. Sreethawong, T.; Ngamsinlapasathian, S.; Yoshikawa, S.; *Mater. Lett.* **2012**, *78*, 135.
61. Kadir, R. A.; Rani, R. A.; Zoolfakar, A. S.; Ou, J. Z.; Shafiei, M.; Wlodarski, W.; Kalantar-zadeh, K.; *Sens. Actuators, B* **2014**, *202*, 74.
62. Sreethawong, T.; Ngamsinlapasathian, S.; Lim, S. H.; Yoshikawa, S.; *Chem. Eng. J.* **2013**, *215-216*, 322.
63. Ou, J. Z.; Rani, R. A.; Ham, M. H.; Field, M. R.; Zhang, Y.; Zheng, H.; Reece, P.; Zhuiykov, S.; Sriram, S.; Bhaskaran, M.; Kaner, R. B.; Kalantar-zadeh, K.; *ACS Nano* **2012**, *6*, 4045.
64. Chen, X.; Shen, S.; Guo, L.; Mao, S. S.; *Chem. Rev.* **2010**, *110*, 6503.
65. Lee, B.; Lu, D.; Kondo, J. N.; Domen, K.; *Chem. Commun.* **2001**, *20*, 2118.
66. Hashemzadeh, F.; Rahimin, R.; Ghaffarinejad, A.; *Ceram. Int.* **2014**, *40*, 9817.
67. Maurer, S. M.; Ko, E. I.; *J. Catal.* **1992**, *135*, 125.
68. Broekhoff, J. C. P.; de Boer, J. H. *J. Catal.* **1968**, *10*, 377.
69. Sing, K. S. W.; *Pure Appl. Chem.* **1985**, *57*, 603.
70. Lin, H-Y.; Yang, H-C.; Wang, W-L.; *Catal. Today* **2011**, *174,* 106.
71. Brandão, R. F.; Quirino, R. L.; Mello, V. M.; Tavares, A. P.; Peres, A. C.; Guinhos, F.; Rubim, J. C.; Suarez, P. A. Z.; *J. Braz. Chem. Soc.* **2009**, *20*, 954.
72. Pereira, C. C. M.; Lachter, E. R.; *Appl. Catal., A* **2004**, *266*, 67.
73. Burcham, L. J.; Datka, J.; Wachs, I. E.; *J. Phys. Chem. B* **1999**, *103*, 6015.
74. Chalmers, J. M.; Griffiths, P. R.; *Handbook of Vibrational Spectroscopy*; Wiley: New York, 2002.
75. Moctezuma, E.; Leyva, E.; Monreal, E.; Villegas N.; Infante, D.; *Chemosphere* **1999**, *39*, 511.
76. Shriver, D. F.; Atkins, P. W.; Overton, T. L.; Rouke, J. P.; Weller, M. T.; Armstrong, F. A.; *Inorganic Chemistry*, 5th ed.; W. H. Freeman and Co.: New York, 2010.
77. Silva, M. K.; Marques, R. G.; Machado, N. R. C. F.; Santos, O. A. A.; *J. Braz. Chem. Soc*. **2002**, *19*, 359.
78. Hashemzadeh, F.; Rahimi, R.; Gaffarinejad, A.; *IJACSR* **2013**, *1*, 95.
79. Raba, A. M.; Barba-Ortega, J.; Joya, M. R.; *Appl. Phys. A* **2015**, *119*, 923.

Submitted: July 28, 2015
Published online: September 18, 2015